Published in Physical Review Letters 45, issue 23, 13579-13590, 1992
which should be used for any reference to this work

Simultaneous analysis of multiple extended x-ray-absorption fine-structure spectra: Application to studies of buried Ge-Si interfaces

P. Aebi, T. Tyliszczak, and A. P. Hitchcock
Institute for Materials Research, McMaster University, Hamilton, Canada L8S 4M1,
and Ontario Centre for Materials Research, McMaster University, Hamilton, Canada L8S 4M1

K. M. Baines and T. K. Sham
Department of Chemistry, University of Western Ontario, London, Canada

T. E. Jackman, J-M. Baribeau, and D. J. Lockwood
Institute for Microstructural Sciences, National Research Council, Ottawa, Canada K1A 0R6

Ge *K*-edge extended x-ray-absorption fine-structure (EXAFS) spectra of a series of strained-layer $[(\mathrm{Si})_m/(\mathrm{Ge})_n]_p$ superlattices grown by molecular-beam epitaxy on the ⟨100⟩ face of single-crystal Si have provided a determination of the degree of intermixing and the extent of relaxation as a function of the thickness of the Ge layer. The results are obtained with use of constrained simultaneous nonlinear least-squares curve fits to multiple data files from different samples. This procedure, along with associated analysis of the fit surface, has improved the reliability of the analysis. We discuss the general applicability of simultaneous analysis procedures to EXAFS analysis of a series of related samples, such as those spanning compositional variation or thermal processing.

I. INTRODUCTION

The extended fine structure in x-ray-absorption spectra (EXAFS) has proven to be a very useful, atom-selective probe of the local geometric structure.[1,2] Although a large amount of information can be deduced from EXAFS spectra, there is as yet no agreed upon optimum analysis procedure. Indeed, it is possible that the best approach varies with the structural problem being investigated. This paper describes procedures we have developed for simultaneous nonlinear least-squares analysis of multiple EXAFS data files that are particularly well suited to studies of a series of related samples. Simultaneous or quasisimultaneous multiple-data-set analysis is used extensively in other spectroscopies, such as reliability-factor analysis of multiple-beam low-energy electron diffraction.[3] However, simultaneous multiple-file analysis of EXAFS is not a standard procedure. While the constrained multiple-file analysis was developed within the context of studies of buried Si-Ge interfaces, the concept should be useful in a wide variety of EXAFS applications. For this reason we give a general exposition and relate it to other recent developments in EXAFS analysis. In addition, we report the results of its application to studies of the structure of Si-Ge interfaces buried in single-crystal Si (Si-Ge superlattice structures).

$\mathrm{Si\text{-}Si_{1-x}Ge_x}$ structures have been used successfully in a number of additional, high-speed devices such as heterojunction bipolar transistors. Interest has grown recently in very-short-period $[(\mathrm{Si})_m/(\mathrm{Ge})_n]_p$ atomic-layer superlattices (ALS) made of p periods of alternating m and n monolayers of *pure* Si and Ge. These materials have been predicted to exhibit optical properties not observed in the bulk or alloy materials due to zone-folding effects.[4] Knowledge of the geometric and electronic structure of ALS samples is essential in order to understand and optimize the growth procedures. Here we report the average Ge-Si and Ge-Ge bond lengths and (Ge,Si) first-shell coordination numbers for a series of superlattices with Ge layer thicknesses between 2 and 8 atomic layers. The change in the distances and coordination numbers provide valuable insights into the transformation from two-dimensional (2D) to three-dimensional growth and the extent of intermixing. The constrained multiple-file analysis was essential in obtaining these results.

II. BACKGROUND

A. SiGe strained layers

There is a 4.2% lattice mismatch between Si and Ge. However, because this is a strongly bonded system, the deposition of pure Ge (or alternatively the codeposition of Si and Ge) onto a Si(100) surface leads to the formation of a strained epilayer. The Ge epilayer adopts the in-plane lattice parameter of the Si(100) template, which results in a tetragonal distortion of the unit cell to accommodate the strain. The intraplanar spacings of alloy layers of varying compositions measured by x-ray diffraction[5] are in agreement with those calculated using classical elasticity theory. The *average* nearest-neighbor distances calculated for strained alloy layers ranging from 0 to 100 % are show in Table I. Growth of strained layers continues until a "critical thickness" is reached, at which point it becomes favorable for the layer to relax.[6]

TABLE I. Average nearest-neighbor distances in $Si_{1-x}Ge_x$ alloys grown on Si.

	Distance (nm)	
x (%)	Strained	Relaxed
0		0.2350
20	0.2363	0.2372
50	0.2381	0.2401
60	0.2387	0.2410
70	0.2393	0.2420
80	0.2400	0.2430
100	0.2412	0.2450

The *average* bond lengths in relaxed alloy samples are also indicated in Table I.

The actual atom-by-atom deposition of pure Ge and the evolution of the growth has been and is still being debated. It is generally agreed that the initial growth is by a Frank-van der Merwe layer-by-layer mechanism (2D) which makes a transition somewhere between three and four monolayers (1 ML is 0.68×10^{15} Si/cm^3) to Stranski-Krastanow mode (3D) islands).[7,8] A recent x-ray-diffraction study[9] has proposed that the critical thickness for strain relief is also 3–4 ML, as opposed to the value of 6 ML determined by ion scattering.[8] The authors attributed the difference to an increased sensitivity to the onset of relaxation. However, Mo *et al.*[10] have studied this transition by scanning-tunnel microscopy and suggest the process may be more complicated than the simple two-stage process indicated above. Relevant to this are the numerous reports of ordering in both SiGe alloys and at Si/Ge interfaces. A wide variety of structural models have been proposed.[11–19] Recently, Copel *et al.*[20] have shown that surfactants can suppress 3D growth and possibly will also prevent the formation of ordered structures. This may provide the means to grow the thicker layers of adequate compositional and interface quality which are needed to achieve recently proposed devices.[21]

The epitaxial layers were grown in a VG Semicon V80 molecular-beam-epitaxy (MBE) system on 100-mm Czochralski (100) Si wafers.[22] To ensure identical initial conditions, a thick Si buffer layer was grown at ≈520 °C using optimum growth conditions. The substrate temperature was then reduced before the thin Si and Ge epitaxial layers were deposited alternately at rates between 0.02 and 0.04 nm/s. For the samples studied, the growth temperature for the layers was 385 °C. Cross-comparisons using Rutherford backscattering, secondary-ion-mass spectrometry, cross-sectional-transmission-electron microscopy, and x-ray-diffraction measurements have established the Ge concentration and nominal layer thicknesses (i.e., ignoring any intermixing).[23,24]

Raman spectra were taken by illuminating the samples with 300 mW of either 458- or 468-nm laser light. Measurements were made in a quasibackscattering geometry,[25] with an incident angle of 77.7° to the sample surface. The scattered light was collected without polarization analysis and dispersed with a SPEC 14018 double monochromator before being detected with a cooled RCA 31034A photo-multiplier. Representative spectra from three ALS samples are shown in Fig. 1.

Raman scattering from longitudinal acoustic and optic phonons in ALS can provide information on interface blurring and intralayer strain,[26,27] as well as give an indication of the overall epitaxial quality.[28] In the best-quality ALS, the folded acoustic modes seen at frequencies below ~200 cm^{-1} have an intensity and linewidth comparable to the higher-frequency optic modes. The Raman spectrum of sample No. 2 ($n\sim2$) shown in Fig. 1 exhibits a strong and narrow folded mode at 182 cm^{-1}, indicating that this sample has sharp interfaces between the nominally pure Si and Ge layers. The positions and intensities of the three optic modes (295, 415, and 513 cm^{-1} in No. 2) are sensitive to the degree of confinement, strain, and interface blurring.[27]

Modeling of the Raman spectrum of No. 1 ($n\sim2$) has been attempted previously.[27] The calculations showed that the degree of mixing at an interface can be estimated. However, without specific information about the disposition of atoms at or near the interfaces, only qualitative results can be obtained. Given that constraint, the degree of intermixing was estimated from the Raman data to be about ~8% at both interfaces.

In the case of the $n\sim4$ ALS (No. 3), the optical phonons are still sharp, but the acoustic mode is generally broader and occasionally weaker (see the peak at 128 cm^{-1}) than for the $n\sim2$ samples, indicating some deterioration in quality. Nonetheless, the layers are still well defined, as indicated by the appearance of another confined Si-layer mode at 496 cm^{-1} below the major Si-layer mode at 514 cm^{-1} in No. 3.

For thicker Ge layers ($n\sim8$), the folded acoustic modes show only weakly in the Raman spectra and are very broad, as can be seen for No. 5 in Fig. 1. The optic mode near 400 cm^{-1} is also broad and weak and, given

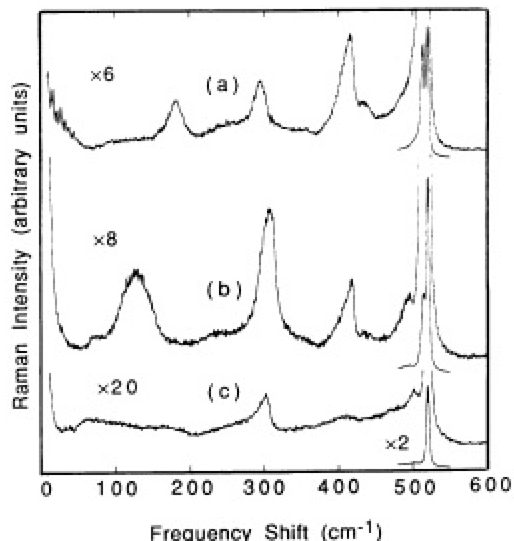

FIG. 1. The Raman spectra of (a) No. 2 ($n\sim2$), (b) No. 3 ($n\sim4$), and (c) No. 5 ($n\sim8$) recorded at a resolution of 3 cm^{-1}. The strong peak at 520 cm^{-1} is due to the Si substrate.

that the frequency and the intensity of this mode are both sensitive to interface blurring,[27] it can be concluded that a greater degree of interface mixing and/or roughness is present than for the thinner layer.

Raman studies of MBE-grown $Si_{1-x}Ge_x$ epilayers and superlattices have shown that two optical-phonon modes near 255 and 435 cm^{-1} can be associated with ordering within the alloy layers.[12] Only a very weak peak was found near 435 cm^{-1} in some of the as-grown ALS and there was no corresponding feature at 255 cm^{-1} (see Fig. 1). This indicates that little if any ordering has occurred at the interfaces in the as-grown material.

B. EXAFS

EXAFS is the energy-dependent interference of the outgoing photoelectron wave created by x-ray absorption above inner-shell (core) ionization thresholds (edges) with that component backscattered from nearby atoms. In a one-particle, single-scattering, harmonic picture[1] the EXAFS signal may be represented as

$$\chi(k)=\sum_i \chi_i(k)=\sum_i A_i(k)N_i/(kR_i^2)\exp(-2k^2\sigma_i^2)$$
$$\times\sin[2kR_i+\delta_i(k)] \ ,$$

where $A_i(k)$ is the backscattering amplitude as a function of wave number ($[k(\text{Å}^{-1})]=[0.263(E-E_0)]^{1/2}$, where E_0 is the photon energy (in eV) at which the photoelectron has zero kinetic energy) from each of the neighboring atoms of type i, which are located at a distance R_i. The EXAFS signal depends not only on the energy (wave number) of the photoelectron and the interatomic distance but also on the number and type of backscatterers in each shell. The type of backscatterer (i.e., its atomic number and, to a smaller extent, the valence-electronic structure) determines the shape of the backscattering amplitude [$A_i(k)$]. $\delta_i(k)$, the phase shift between the outgoing and backscattered components of the photoelectron wave function, depends on the identity of both absorber and backscatterer. The experimental amplitude is attenuated by inelastic scattering (λ, the mean free path) and by thermal motion and static disorder, which enter into this expression as σ^2, the mean-square relative displacement along the absorber-backscatterer direction (the EXAFS Debye-Waller factor, also denoted by DW in this paper). This expression assumes Gaussian distributions of interatomic distances and does not explicitly account for inelastic and multiple-scattering intensity losses, although these are largely accounted for when experimental models are used in the analysis.

Detailed prescriptions and accompanying rationalizations have been presented for EXAFS analysis within the plane-wave-based, single-scattering, Gaussian distance distribution model.[1] Standards and criteria for such analyses have been established.[29] In situations where a coordination shell (usually the nearest neighbor) consists of a single element isolated from any other component, the structural parameters can be derived from an analysis of the Fourier filtered data using appropriate calculated or experimental phases and amplitudes. Recently, much-improved spherical-wave[30,31] calculations have supplanted earlier plane-wave[32] calculations, allowing the use of data lower in the core-ionization continuum, which is very helpful when dealing with low-Z backscatterers. Several procedures have been developed to optimize these analyses, including criteria for automatic background removal,[33] selection of data range,[34] and the choice of E_0 (the k-scale origin) through phase linearization.[1,35,36] In some cases, such as highly disordered or weakly bonded materials where one needs to go beyond the assumption of a Gaussian distribution, the formalism has been extended through the use of either analytical radial-distribution functions or cumulant techniques.[37] For systems involving heavy atoms where structured backscattering amplitude and phase functions often make the standard analysis ill conditioned, incorporation of the phase and/or amplitude in the Fourier analysis can clarify the interpretation and more reliably reveal low-Z components in the presence of high-Z components.[38] Recently, procedures to calibrate EXAFS using powder x-ray diffraction data recorded under anomalous dispersion conditions have been developed.[39] Other themes in EXAFS data analysis have been described recently by Crozier.[40]

In cases where a single "structural shell" contains several components (as defined by overlapping peaks in an EXAFS radial distribution function), these approaches are inadequate and a nonlinear least-squares curve fit analysis in wave number[1] or energy[41] space is required. In those cases where there is sufficient data range to detect beating between the two components, the beat frequency gives the difference in the two distances.[42]

In many applications EXAFS is used to study trends through a series of closely related samples, such as the annealing of materials,[43] variable composition alloys,[44] oxide glasses,[45] solutions of variable composition,[46] etc. In these situations, many parameters should either be identical (e.g., E_0) or exhibit systematic trends through the series. If the EXAFS spectra of each sample is analyzed independently, it is difficult to take advantage of physically reasonable constraints on the values of structural parameters over the series. We have developed a procedure for flexible, constrained, simultaneous nonlinear least-squares analysis of a number of EXAFS data files. This represents a significant improvement over previously discussed procedures to combine information from several different sources in EXAFS analysis, such as the "fine-adjustment-based-on-models" procedure of Teo, Antonio, and Averill.[47]

C. Application of EXAFS to studies of Si-Ge interfaces

Given the intense interest in quantum-engineered materials containing Si-Ge interfaces, it is not surprising that other Ge K EXAFS studies have been carried out. Oyangi *et al.*[48] have used fluorescence detection in a total-reflection geometry in a "tour-de-force" study of a single monoatomic epitaxial Ge layer, as well as other studies of the layer thickness dependence of $Si/Ge_n/Si(100)$. Bouldin and co-workers have reported

studies of Ge-Si alloys prepared by implantation[49] or by MBE.[5] We have made preliminary reports of our EXAFS studies of single and multiple Ge layers,[50] comparisons to Raman and single-crystal x-ray-diffraction measurements.[23] A study of interdiffusion in a $[(Si)_8/(Ge)_2]_{100}$ sample as a function of annealing time[51] is being reported in a separate paper. The principle motivation of our Ge *K* EXAFS studies is to better understand interdiffusion and intermixing during growth and postgrowth processing (annealing and other fabrication steps) from a local-structure viewpoint. Thus, our interest is focused on how structural parameters change as a function of growth or annealing procedures. The constrained multiple-file analysis provides absolute accuracies at least as good as, and probably better than, independent analysis. Most importantly, it provides much-improved accuracy of the *relative* values, i.e., trends through a series of related samples.

The ALS materials present particular challenges for EXAFS since some Ge atoms (those inside a Ge layer) will have only Ge neighbors, others (those at the interface) will have both Si and Ge neighbors, and still others (those which have migrated into the Si layer) will have mainly Si neighbors. Since the measured EXAFS is a weighted average over all Ge environments, the first-shell analysis only provides an averaged Ge-Si and Ge-Ge distance (R), coordination number (N), and Debye-Waller factor (σ^2 or DW). In addition, the Ge-Si and Ge-Ge signals cannot be separated on the basis of distance, i.e., the first shell consists of two unresolved components. In the pure materials the nearest-neighbor distances for Si and Ge are 0.235 and 0.245 nm, respectively. Amorphous and single-crystal alloys of Si and Ge have intermediate nearest-neighbor spacings.[52–55] Thus, one expects the Si-Si, Ge-Ge, and Si-Ge bonds at the epitaxial interface to have intermediate bond lengths. Therefore, we are necessarily looking at changes close to (or even below) the limits of absolute errors in conventional EXAFS analysis. These challenges were the motivation for developing the multiple-file analysis procedure.

III. APPLICATION TO ALS

A. Procedure

The EXAFS signal must be extracted from the raw x-ray-absorption spectrum as measured by conventional transmission, or (as in this case) by electron or fluorescence yield. This involves setting the energy scale to zero at the half height of the edge jump, transforming from energy to **k** space with k^1 multiplication, then subtracting the nonoscillatory background generated by fitting the continuum data over a standard range to a multisection polynomial spline function (three equal-section cubic splines were used in this work). EXAFS signals corresponding to particular shells are isolated using Fourier filtering. Quantitative structural parameters relating to this signal are then derived using curve fitting based on backscattering amplitudes and phases for the individual components obtained either from analysis of experimental spectra of model compounds or from spherical-wave calculations.[30,31]

In any EXAFS analysis it is important to investigate the dependence of the result on the background subtraction and the range of forward and reverse Fourier transforms. In many cases, apparently small variations can cause significant changes in the shape and the position of the maximum of the amplitude function, and even in node locations, upon which the interatomic distances are directly related. It is difficult to define a fail-safe recipe for the optimum procedure to convert raw spectral data to the Fourier-filtered $\chi(k)$ data used as input to the curve-fit analysis. Even so, it is critical to use rigorously identical procedures for model data as well as all sample data. In the present analysis we have found that the background subtraction and the range of reverse transform (ΔR) are particularly sensitive aspects of preparation of the Fourier-filtered files. The ranges in **k** and **R** space define N_{expt}, the number of degrees of freedom of the data, i.e., the number of truly independent experimental points:[56]

$$N_{\text{expt}} = 2\,\Delta k\,\Delta R/\pi\ .$$

We emphasize that consideration of the number of degrees of freedom gives a necessary, but not necessarily a sufficient, condition for producing meaningful results. Increasing ΔR increases N_{expt} but there is always uncertainty about including contributions from other shells, especially in materials with many different local environments of the absorber. Using the maximum possible k range is also desirable to give maximum precision. The k range is limited at high k to the point at which the real EXAFS signal becomes indistinguishable from the noise (usually being limited more by systematic than by random noise). While in principle the minimum k value could be taken as the edge jump, in practice it is limited to several Å^{-1}, in order to avoid distortions associated with the strong near-edge multiple-scattering signal, as well as difficulties in background subtraction in regions of rapid signal variation. The availability of good experimental models and spherical-wave calculated phases and amplitudes,[30,31] including some consideration of multiple scattering,[31] has allowed the reduction of typical k_{min} values from 4 to 2 Å^{-1}.

After background subtraction over an appropriate k range, which includes k^1 weighting and normalization to the nonoscillatory portion of the continuum (μ_0, which we approximate from the experimental data as the difference in linear fits to the preedge and postedge data), it is Fourier transformed without apodization. Our choice of k^1 weighting is at variance with the common EXAFS practice of using k^2 or k^3 weighting to "symmetrize" the peaks in the Fourier transform (FT) by making the backscattering envelope more Gaussian in shape.[1,32] We find that higher k weightings cause loss of low-k information. This is a real disadvantage, particularly when one is dealing with a relatively low-Z backscatterer like Si whose amplitude envelope peaks at 4 Å^{-1}. In our experience, analysis with high k weighting usually leads to a distortion of the relative coordination numbers for low- and high-Z components.

The next important decision in the analysis is the window and apodization for the reverse transform (Fourier filtering). A symmetric Hanning apodization with taper over 30% of the window was used in this work. With the less symmetric peak shapes that occur with multicomponent shells and k^1 weighting, one must be careful to include all parts of the FT relevant to the shell of interest. For example, the FT of the $n=2$ data in Fig. 2 has a very steep decline at 2.2 Å. This decline does *not* signify the end of the first shell; rather, it is a consequence of the overlap of the Si and Ge components. The secondary peak at 2.4 Å is very much part of the first-shell signal and must be included in the reverse transform if one wants to correctly evaluate the mixture of Si and Ge neighbors in the first shell. At the same time, one does not want to choose too wide a filter window. On the high side, this can lead to inclusion of the second-shell signal. On the low side, especially below 1 Å, one can add signal which is really a consequence of residual background. At the same time, complex backscattering amplitude shapes and component interferences can lead to a real low-R shoulder or tail which must be included. In this context we find it very useful to examine the shape of the FT of the signal calculated using spherical wave phases and amplitudes,[31] since we find this to be a good predictor of the complexities leading to non-Gaussian peaks in FT magnitude spectra.

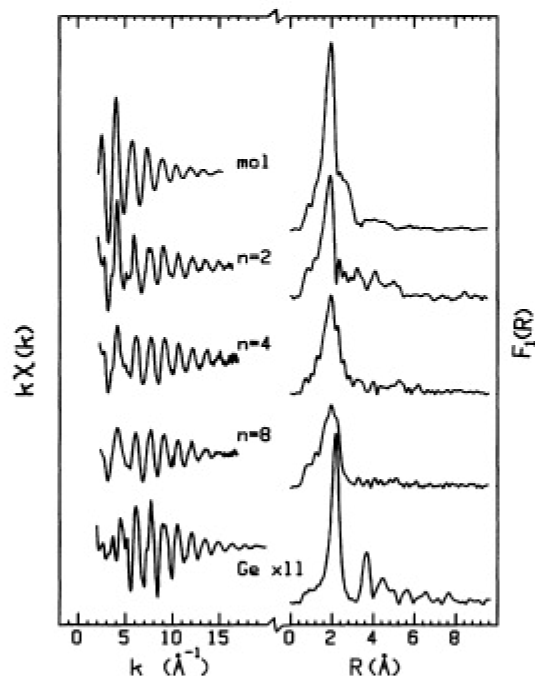

FIG. 2. $k\chi(k)$ Ge K-edge EXAFS (left) and magnitude of the Fourier transforms (right) for $[(Si)_m/(Ge)_n]_p$ ALS structures MBE grown on single-crystal Si(100). The target values of (m,n,p) for the $n=2$, $n=4$, and $n=7$ ALS samples were (8,2,100),(9,4,24), and (20,7,8). Table II lists m and n values measured by x-ray diffraction. The results for single-crystal Ge (Ge×11, the Ge-Ge model) and solid $Ge[Si(CH_3)_3]_4$ (mol, the Ge-Si model)[60] are also shown. The spectra were recorded at room temperature using total electron-yield detection with a rotating gas ionization detector.[59]

The Fourier-filtered first-shell signal is then fit to an appropriate model. In order to carry out the curve-fit analysis, backscattering amplitudes and phases are needed.[1] Exactly the same file-preparation procedures should be applied to extract phases and amplitudes from experimental measurements of suitable model compounds or from theoretical calculations. Treating data and models equally increases the chance of cancellation of systematic distortions due to background subtraction and Fourier filtering procedures.

Presently we can simultaneously analyze up to four spectra, each of which has up to four components. While it would be a relatively simple matter to extend this to a larger number of data files and a larger number of components, the computational times would increase significantly. Usually one analyzes several different sets of spectra, which has the advantage of testing the uniqueness of any one set. If the same spectra were fit independently, the four parameters (R, N, DW, and E_0) for each of the two first-shell components would result in eight fit parameters for one spectrum with two components, giving 32 fit parameters overall for an unconstrained analysis of four spectra. With the multiple-file analysis one can selectively reduce the number of free parameters in a physically meaningful way. In our analysis of the Ge K EXAFS of these ALS samples we have chosen to require that the E_0 and DW parameters for each component are identical for each of the four spectra. This choice reduces the number of independent parameters from 32 to 20. A common E_0 is a reasonable assumption in many cases, since E_0 approximates the average potential along the internuclear distance,[1,2] which should be approximately the same for a given pair of elements in slightly different environments. Since the E_0 value for any file is also dictated by the calibration of the original energy scale, it is essential that this calibration be done identically for all spectra. The assumption of a common DW factor is probably less general but we believe it to be appropriate in this case because, in these epitaxial, single-crystal samples, each Ge atom should have four relatively rigid bonds with a small and harmonic thermal motion. In other applications it may be appropriate to constrain other parameters. For example, if one analyzed a series of spectra of the same material recorded at different temperatures, then one would want to assume identical E_0, N, and perhaps R, but different DW factors.

Although we have used a two-component analysis in this illustration of our procedure, there are many cases where a constrained multiple-file curve-fit analysis would be much better than a spectrum-by-spectrum analysis even for well-isolated one-component shells because of the increase in reliability associated with the introduction of physically meaningful constraints.

An additional aspect of our analysis procedure is a systematic investigation of the contours of the fit surface. We systematically vary the starting point of the fit by scanning initial parameters over selected ranges (typically, one scans initial values only within a physically significant range). For each set of initial parameters the

fit is carried out to a predefined convergence limit. By starting from a large number of initial parameters one can learn a considerable amount about the fit surface and thus the quality of the derived parameters. By plotting values of the parameters against each other for the whole sequence of scanned fits one can investigate either the correlation of end parameters among each other, or the dependence of the final result on the initial parameters of the fit. Trends in R or N through different samples are detected very clearly when using scans of initial parameters in conjunction with the multiple-file fits, since parameter correlations are easily observed and the scatter of the fits gives a very direct measure of the relative errors.

B. Results

The Ge K EXAFS spectra were recorded at the $A3$ and $C2$ beam lines at the Cornell High Energy Synchrotron Source (CHESS). Electron-yield detection[57,58] allows study of the local environment of atoms near the surface (<0.1 μm) because of the limited escape depth of the Auger and secondary electrons produced in the decay of the core hole. A special gas-flow electron detector with sample rotation[59] is used in order to eliminate diffraction artifacts while providing gas amplification of the electron-yield signal. Typical acquisition times were 20 min per spectrum. Two to four spectra were summed to generate the file subsequently analyzed. The EXAFS spectrum of the Ge single crystal recorded with the gas ionization detector with sample rotation was identical to that of powdered Ge recorded in a conventional transmission measurement, indicating that the statistical quality is excellent and that smooth rotation in a single plane effectively eliminates diffraction structure.

Figure 2 shows a selection of EXAFS spectra [$\chi(k)$] for two model compounds, single-crystal Ge and $Ge[Si(CH_3)_3]_4$, as well as a series of buried Si-Ge superlattices with Ge layers of different thicknesses (see the figure caption for description of the samples). All EXAFS data were extracted from spectra which were recorded at room temperature with total electron-yield detection using the rotating gas ionization system.[59] A uniform, fine-particle film of the $Ge[Si(CH_3)_3]_4$ was prepared by evaporation from an acetone solution. Figure 2 also plots the magnitude of the Fourier transform of each EXAFS spectrum. The Ge K spectra of pure single-crystal Ge (bottom curve of Fig. 2) was used to provide experimental Ge-Ge phase and amplitude model functions, while that of the molecular compound, $Ge[Si(CH_3)_3]_4$ (Ref. 60) (top curve of Fig. 2), was used for the Ge-Si model functions. In each model species there is a well-isolated first shell which consists of only Ge and only Si nearest neighbors, respectively (the shoulder around 2.8 Å in the FT of the molecular compound corresponds to the Ge-C distance). The Ge-Ge distance in pure Ge (0.2450 nm) is well known. The crystal structure of $Ge[Si(CH_3)_3]_4$ has not yet been determined. We have assumed its Ge-Si bond length to be 0.2389 nm based on the values of 0.2384(1) nm in triphenylgermanium-trimethylsilicon [$(C_6H_5)_3Ge\text{-}Si(CH_3)_3$] and 0.2394(1) nm in trimethylgermanium-triphenylsilicon [$(CH_3)_3Ge\text{-}Si(C_6H_5)_3$], as determined by single-crystal x-ray diffraction.[61] Uncertainty in the Ge-Si bond length of the model compound would affect the accuracy but not the precision of our results. The maxima of the backscattering envelopes for Si and Ge are located at different positions (4 Å^{-1} for Si and 8 Å^{-1} for Ge). The height of the EXAFS signal at $k=4$ Å^{-1} provides an easy qualitative measure of the amount of first-shell Si since the Ge backscattering amplitude is almost zero at that value.[50]

The relatively broad main peak (1–3 Å) in the FT's of the ALS samples indicates that there are several components (i.e., Si or Ge nearest neighbors with different distances) within the first shell. Therefore, quantitative analysis must involve a curve-fitting procedure. We have chosen to carry this out in **k** space on the Fourier-filtered first-shell data, rather than **E** or **R** space. The k range for our data analysis is 2.4–14.8 Å^{-1}, while the R range of the Fourier back transform is 1.2–2.6 Å, giving $N_{expt}=11$. These values were chosen according to the criteria discussed in the preceding section. The Fourier-filtered first-shell data for four samples are simultaneously fit to an appropriate model, in this case consisting of two components, which give the position (R), number (N), the mean-square relative displacement (DW) of the Ge and Si neighbors, averaged over all sites.

Figure 3 illustrates the quality of a constrained two-component fit to four Fourier-filtered first-shell Ge K EXAFS spectra: the as-grown $[(Si_8\text{-}Ge_2]_{100}$ sample, and

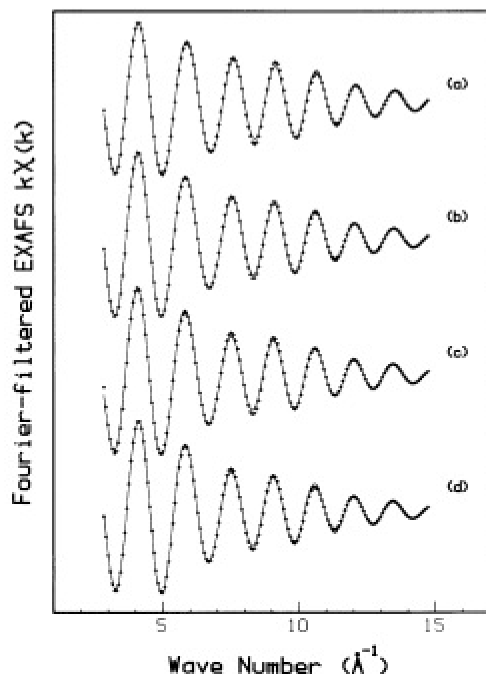

FIG. 3. Example of the quality of a fit to a Fourier-filtered Ge K-edge EXAFS spectrum based on simultaneous analysis of (a) the as-grown $[(Si)_8/Ge_2]_{100}$ sample, and after (b) 20 s, (c) 200 s, and (d) 2000 s anneal at 750 °C. The models used were single-crystal Ge and $Ge[Si(CH_3)_3]_4$ analyzed in a strictly identical fashion. See Ref. 51 for quantitative results and interpretation.

the same sample after 20, 200, and 2000 s thermal anneals.[51] Visually, it is clear that the quality of the raw data (Fig. 2) and the fit to the Fourier-filtered data (Fig. 3) are both excellent. The quality of fit can be quantified through χ^2, derived in the nonlinear least-square-fitting procedure. However, one soon realizes that one can produce fits of visually indistinguishable quality and similar χ^2 but with clearly unphysical parameters. Hence, another criterion is, how reasonable are the parameters produced by the fitting. Even within the range of "reasonable physical parameters" there may be several different fits with almost the same χ^2. Which is the best one to choose? The number of minima of similar depth in the χ^2 surface can be reduced either by increasing the data range or by reducing the number of free parameters, i.e., constraining certain parameters to have the same value in a number of data sets. Both procedures result in better stability with respect to different starting parameters. A logical step to increase stability is to reduce the total number of parameters per unit data range (i.e., $N_{par}/\Delta k$). This can be done by simultaneously fitting a number of different spectra with certain parameters constrained to have the same value in each file.

Another way of increasing the information content in the analysis is to measure the same sample at different temperatures and then to fit different files together with common E_0 and N. So far we are only able to record the EXAFS spectra of these single-crystal Si-Ge samples at room temperature because of the necessity of sample rotation and electron-yield detection to remove crystal diffraction artifacts.[57-59] Alternatively, spectra recorded in different polarizations may provide additional degrees of freedom. From our studies to date there appears to be relatively little polarization dependence of the EXAFS first-shell signal.[50] This is as expected because the local Ge environment is only slightly distorted from tetrahedral. In a perfect tetrahedral environment all four bonds are sampled equally in all orientations. The present analysis does not explicitly take into account polarization effects.

The simultaneous analysis of related samples with appropriate constraints has two beneficial effects. First, it makes the fit more stable and it provides more precise values of the differences in structural parameters for a series of closely related spectra and/or samples. The mathematical techniques used in EXAFS analysis provide estimates of the random errors. However, systematic errors are often several times larger. Sources of these include a relatively strong dependence of the final result on choices made in the EXAFS data file preparation and Fourier analysis, systematic errors associated with terms neglected in the EXAFS model employed (e.g., approximating the distance distribution as a Gaussian), and the uncertainty in the decision of what constitutes the correct structural model. In EXAFS there are two pairs of highly correlated parameters, i.e., (R, E_0) and (N, DW). In independent analyses of individual files, this correlation can play havoc with extraction of correct values for the individual parameters. Second, the introduction of physically reasonable parameter constraints reduces these correlations and increases the chances of deriving the true answer. In addition, examination of the fit surface through systematic scans of the initial parameters and subsequent graphical analysis provides alternative approaches to error estimation that can be very useful in building confidence in the results.

We have used a scanned multiple-file analysis in order to explore the contours of the Ge-Si fit surface (a 20-parameter space in this case). The initial parameters of the four files of the fit series were scanned together in nested loops: $R_{\text{Ge-Ge}}$ and $R_{\text{Ge-Si}}$ were varied from 2.36 to 2.43 Å in three steps (this range is dictated by the bond lengths in bulk Si and Ge, along with observations in alloys[52-55]); N_{Ge}—the number of Ge neighbors—was varied from 1.2 to 2.8 in three steps, while setting the initial N_{Si} to 4-N_{Ge} (i.e., normalizing N_{initial} to the total number of neighbors in a tetrahedral environment); and $E_{0_{\text{Ge}}}$ and $E_{0_{\text{Si}}}$ were each varied independently from -5 to 5 eV in six steps. The initial values of $\Delta\sigma^2$, the DW parameter, were always zero because these values are relative to the experimental models which should have comparable thermal motion factors. Overall, this scan procedure involved 972 ($3\times3\times3\times6\times6$) different initial conditions for which converged fits were carried out. Each fit takes between 10 and 50 iterations and each iteration takes about 2 s of CPU time on an IBM PS/2 Model 70 computer (Intel *i*486 processor), running at 25 MHz. Examination of initial and final parameters, together with the χ^2 for each fit, provides many ways to investigate the behavior of the fit. Figures 4–7 show examples of how this data base has been manipulated to graphically explore the fit surface and answer specific questions about the fitting.

Figure 4 plots the Ge-Ge and Ge-Si distances versus χ^2 for a series of converged fits for the $[(\text{Ge}_2\text{-Si}_8)]_{100}$ sample, starting with systematically different initial parameters. Plots of this type explore the local fit surface, graphically present the scatter of the optimized parameter values, and allow an average parameter value and standard deviation to be calculated from the best fits. This gives a measure of the sharpness of the minimum. In the particular example of Fig. 4, one notes that the scatter, as well as the width of the "hole" in the fit surface, is larger in the $R_{\text{Ge-Si}}$ than the $R_{\text{Ge-Ge}}$ dimension. This was a general observation in the analysis of all of the sets of Si-Ge samples. Since the Ge-Ge bonds are predominantly in the Ge layer, while the Ge-Si bonds can be distributed between the interface and Ge that has diffused into the Si layer, the broader $R_{\text{Ge-Si}}$ minimum may be a reflection of a wider distribution of Ge-Si sites.

Figure 5 is a histogram derived from the scanned fits to the first-shell Ge K-edge data for four $n=2$ samples as grown and annealed for 20, 200, and 2000 s.[51] It is the number density of final values (i.e., χ^2 the number of fits which end with χ^2 in the indicated interval) over all of the initial parameters explored. Figure 5 shows that most initial conditions within the physically reasonable parameter range result in the minimum χ^2, giving confidence in the uniqueness of the converged fit. This result is more pronounced the more stringent a convergence criterion that is used for the least-squares fit. At

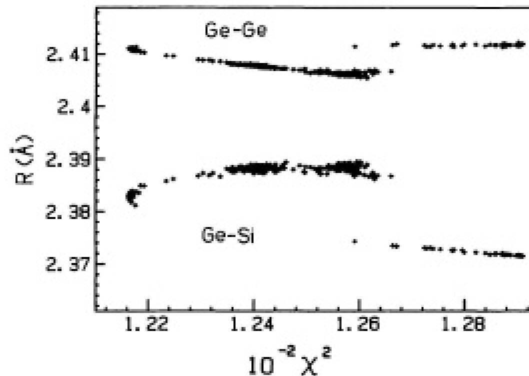

FIG. 4. χ^2-fit parameters from converged fits vs the Ge-Ge and Ge-Si distances predicted for a $[(Ge)_2/(Si)_8]_{100}$ as-grown sample in the as-grown, 20, 200, and 2000-s anneal series. Such plots are useful in evaluating the fit surface and estimating the precision of the results.

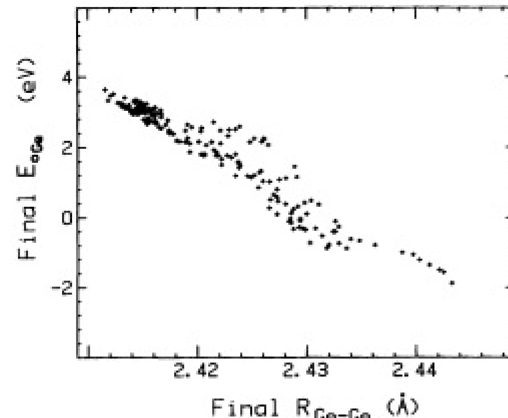

FIG. 6. Plot of the relationship between the k-scale origin (E_0) and the Ge-Ge distance derived from a range of converged fits. Plots of this type can be made between any pair of parameters to investigate the degree of correlation between parameters.

$\epsilon=1.0\times10^{-6}$ (ϵ is the convergence parameter, the difference in χ^2 on successive steps in the fit) (upper curve), twice as many fits find their way to the lowest value than at $\epsilon=1.0\times10^{-3}$ (lower curve). In an analogous fashion the distribution of fits relative to any initial parameter, e.g., R(Ge-Si), can also be plotted.

Figures 6 and 7 provide examples of graphical analysis used to investigate the correlation of parameters and the dependence of the final result on the initial parameters of the fit. Figure 6, a plot of $R_{Ge\text{-}Ge}$ for the as-grown $n=2$ sample against E_0(Ge), the inner potential term for the Ge-Ge component, shows that these two parameters are highly correlated. Since this is a common E_0 for all files, this correlation of R and E_0 makes it essential that all the

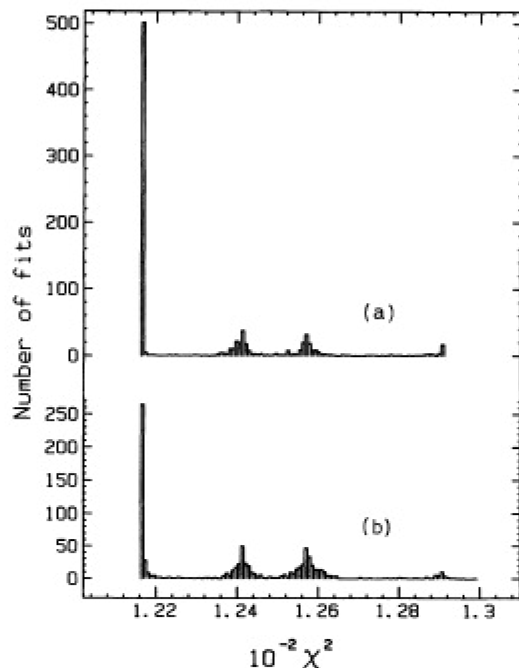

FIG. 5. Histogram of the number of fits with a given χ^2 for the series of initial parameters noted in the text. (a) corresponds to a convergence criterion (difference in χ^2 in successive steps), $\epsilon=10^{-6}$ while (b) corresponds to $\epsilon=10^{-3}$. As ϵ is reduced, a larger number of initial parameter combinations converge to the region of the best fit.

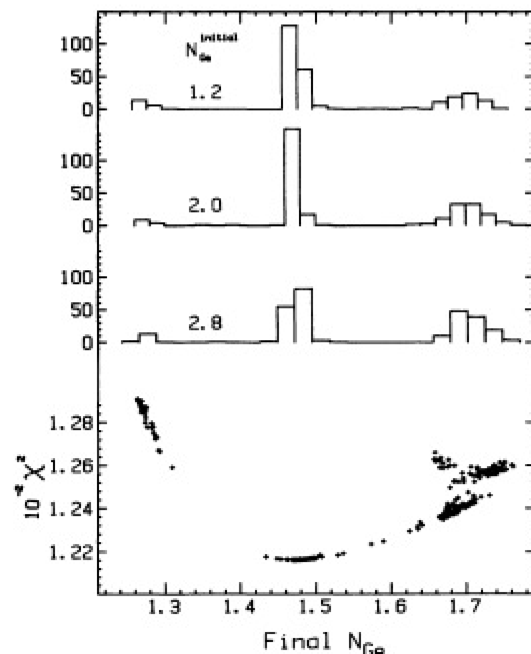

FIG. 7. Histograms of the number of fits yielding particular final Ge-Ge coordination numbers starting from various initial parameters, as discussed in the text. The three top curves correspond to series of initial parameters, each with a different initial value of N_{Ge} in the fit. The bottom curve shows the χ^2 distribution over the same ordinate range. Plots of this type can be made to investigate how the final value depends on its initial value for any parameter.

files within a fit series are calibrated identically. In this case, the slope (dR/dE_0) is about 0.5 pm per eV for $R_{Ge\text{-}Ge}$ between 0.241 and 0.242 nm, the range of the minimum χ^2, i.e., the best fits.

Figure 7 is a histogram for the as-grown $n=2$ sample (taken from a fit to the $n=2$ anneal data[51]) of the number of fits which produce a given N_{Ge}, starting with three different initial N_{Ge} values. Again, one sees that the minimum of χ^2 and the most frequent final N_{Ge} value coincide. Plots of this type indicate that no matter what initial parameters are chosen (at least within physically reasonable values), the fit most frequently converges to the same minimum χ^2 answer. The same point can also be made by plotting initial parameter values against χ^2 to see that good χ^2 values result starting from a wide range of initial parameters. Many such plots can be (and were) made in order to investigate the behavior of the fitting.

Since (at present) only four files are treated simultaneously, but there are more than four samples in each series, we have used overlapping sets of files to span the full data set. The optimized fit parameters for the same file in different data sets are slightly different. The degree of consistency of these repeat analyses is another test of the accuracy of our curve-fitting EXAFS analysis procedures. This, along with investigations of the fit behavior with other model functions, provides a means of estimating absolute errors in the determination of the parameters in the EXAFS model.

C. Discussion

Table II shows the values of $R_{Ge\text{-}Ge}$, $R_{Si\text{-}Ge}$, and the ratio of nearest neighbors $N_{Si\text{-}Ge}/N_{Ge\text{-}Ge}$ derived using the analysis described above from the Ge *K* EXAFS of a set of six ALS grown without the use of surfactants). These samples have been the basis of continuing studies by a wide range of techniques and are rather well characterized. The present results demonstrate that EXAFS can provide quantitative information which supplements that from other short-range probes (e.g., Raman), or from diffraction techniques.

First, consider the two $n\sim 2$ samples. Figure 8 presents some sketches of possible interface configurations. In the ideal $n\sim 2$ interface [Fig. 8(a)] $N_{Si\text{-}Ge}/N_{Ge\text{-}Ge}$, the ratio of bonds, is 1.0 [in the general case, the value for a perfect Ge_n layer is $1/(n-1)$]. Any deviation from the perfect interface, such as the random displacements depicted in sketch 8(b), will increase $N_{Si\text{-}Ge}/N_{Ge\text{-}Ge}$. Thus, the measured $N_{Si\text{-}Ge}/N_{Ge\text{-}Ge}$ value is a direct indication of the amount of intermixing. Quite clearly, the observed bond ratio for the $n\sim 2$ samples [1.4(1), Table II] is inconsistent with previously proposed models [Fig. 8(c), based on Refs. 13 and 14; Fig 8(d), based on Refs. 11 and 15] for ordered bulk Si-Ge alloys which might have been considered relevant models for these interfaces. On the other hand, the observed bond ratio is consistent with the *absence* of any significant intensity in the Raman spectrum of vibrational modes at 255 and 435 cm^{-1}, which have been attributed to "ordering."[12] If we assume that intermixing occurs at both interfaces,[15] then the observed $N_{Si\text{-}Ge}/N_{Ge\text{-}Ge}$ values of 1.35 and 1.43 for the $n\sim 2$ samples correspond to ~20% mixing in both layers [Fig. 8(b)]. However, if we assume that the mixing occurs predominantly during the deposition of Si onto Ge (Ref. 16) (as opposed to Ge onto Si), then we would have ~40% intermixing at the Si→Ge interface, in agreement with a recent model.[62]

Our measured Si-Ge and Ge-Ge bound lengths are substantially different from each other, as has been proposed recently[63] and observed by both Si *K* and Ge *K* EXAFS measurements of crystalline and amorphous Si-Ge alloys.[52–55] The value of $R_{Ge\text{-}Ge}$ in the $n\sim 2$ samples is in good agreement with that calculated for a fully strained pure Ge layer, as expected. The value of $R_{Ge\text{-}Si}$ in the $n\sim 2$ samples (0.239 nm) is very similar to that of 0.238 nm found by Oyangi *et al.* for a SiGeSi heterostructure.[48] It is close to the average bond length for a strained 60% alloy (Table I). This is not surprising, since the Si-Ge bond length dominates the average bond length for alloys at compositions near 50%. Obviously, the distances given in Table I are the *average* interplanar distances, representing the weighted average of the Si-Si, Si-

TABLE II. Structural parameters derived from curve-fit analysis of the first-shell EXAFS of $[(Si)_m/(Ge)_n]_p$ epitaxial superlattices. (Derived using simultaneous fits to several subsets of four files. E_0 and DW for each component were constrained to be the same in all four files in order to reduce the number of parameters from 32 to 20 for each set of four files.)

Sample Code	m[a] (ML)	n[a] (ML)	p	$R_{Ge\text{-}Ge}$(nm) (±0.0005 nm)[b]	N_{Ge}	$R_{Ge\text{-}Si}$(nm) (±0.0005 nm)[b]	N_{Si}	$N_{Ge\text{-}Si}/N_{Ge\text{-}Ge}$
No. 1	6.6	2.0	48	0.2410	1.65	0.2396	2.25	1.35±0.15
No. 2	8.0	2.2	100	0.2413	1.70	0.2388	2.45	1.43±0.10
No. 3	9.3	3.7	24	0.2403	2.40	0.2394	1.60	0.61±0.03
No. 4	6.9	3.7	15	0.2409	2.55	0.2401	1.45	0.58±0.03
No. 5	20.0	8.0	8	0.2422	2.70	0.2412	1.30	0.48±0.03
No. 6	17.5	8.7	8	0.2424	2.80	0.2439	1.20	0.40±0.03

[a]As measured by double-crystal x-ray diffraction and $\theta-2\theta$ measurements.

[b]Uncertainty in changes of bond lengths from sample to sample and from $R_{Ge\text{-}Si}$ and $R_{Ge\text{-}Ge}$ in the same sample. This is estimated from the stability of the fit and sample-to-sample variations. The absolute uncertainty of EXAFS distance determination is generally assumed to be 0.002 nm (see text for further comments).

Ge, and Ge-Ge bond lengths in an epitaxial layer[63] or alloy sample. The very reasonable values of both the Ge-Si and Ge-Ge bond lengths in the $n \sim 2$ samples determined by our EXAFS analysis strongly suggests that our absolute accuracy for bond-length determination is actually close to what we have quoted as a precision in Table I, rather than the usually adopted value of 0.002 nm.

The $n \sim 4$-ML samples are similar to the $n = 2$-ML samples in that the bond lengths measured by EXAFS are essentially the same. This is a clear indication that the layer is still strained and growing two dimensionally (as expected and discussed above). Within the precision of the present measurement, the amount of mixing (as measured by the increase in number of Si-Ge bonds) is the same as for $n \sim 2$. Therefore, we would seem to have a continuation of either $\sim 20\%$ mixing in the first and fourth layers deposited, or 40% in the fourth layer. We do not observe the same amount of mixing throughout the four layers, as was observed "throughout" the previous two layers. This is consistent with the Raman results, which indicated that the $n \sim 4$ ALS have interfaces of comparable quality to the $n \sim 2$. It is clear, though, that EXAFS (as with any short-range probe) cannot make predictions about long-range ordering. As mentioned earlier, it is really through monitoring systematic changes (such as the annealing study[51]), or providing a check on models which invoke long-range order, that EXAFS has a role to play. In this context, further EXAFS analysis is most likely to be productive if it is integrated with microscopy- or diffraction-based measurements.

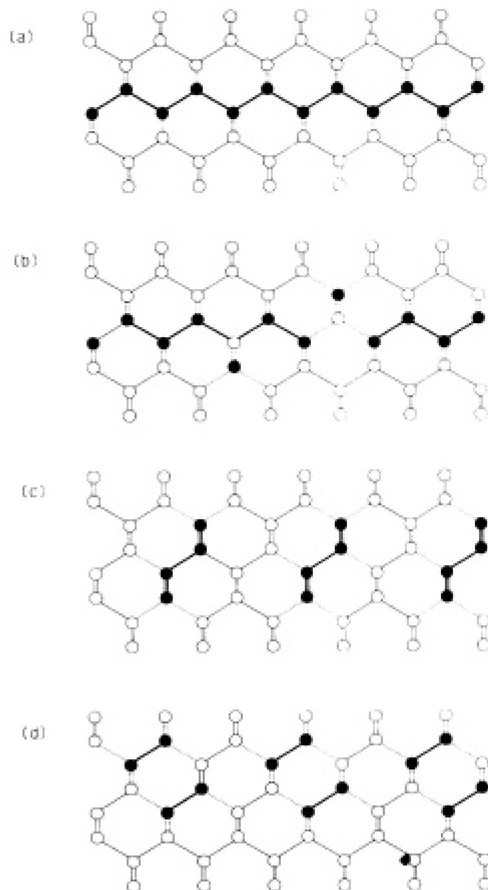

FIG. 8. Schematic of possible configurations for a nominal 2-ML Ge layer in Si. (a) Perfect ALS structure. (b) Random mixing at both interfaces. (c) Ordering proposed on the basis of bulk alloy studies (Refs. 13 and 14). (d) Ordering proposed based on the basis of diffraction studies (Refs. 11 and 15). In the figure, bold lines indicate Ge-Ge bonds, normal thickness lines indicate Si-Si bonds, and dashed lines indicate Ge-Si bonds. Double-line connections indicate out-of-plane nearest-neighbor contacts. The bond lengths for the as-grown $n = 2$ ALS structure are given in Table II. The (a) Ge-Ge interplanar distance and the (b) Ge-Si interplanar distance are not equal.

As expected, the $n \sim 8$-ML samples, which are above the critical thickness for relaxation, were significantly different. $R_{\text{Ge-Ge}}$ has increases substantially, which is consistent with a movement towards a relaxed Ge-Ge bond length of 0.245 nm. Because we average over all Ge-Ge bond lengths, we cannot tell whether the entire layer has a strain consistent with this value (partial relaxation of the whole layer) or different parts of the layer have different strains (and, therefore, different bond lengths). The value of $R_{\text{Si-Ge}}$ is even less straightforward to interpret. We know that significant interdiffusion has accompanied the relaxation, as the bond ratios are larger than would be predicted by extrapolation of the $n \sim 2$ and $n \sim 4$ data. This means we potentially have Si-Ge bonds in a variety of compositional and strain environments. Again, these conclusions are supported by the Raman results for the $n \sim 8$ sample, where the extreme breadth of the acoustic modes and one optic mode indicates that there must be a wide variety of environments of the Si and Ge atoms across the interface. To understand the results fully, we will have to follow n over a much finer scale and support the interpretation with electron microscopy images. However our studies so far convince us that EXAFS can provide information not readily accessible by any other means, which will be critical to testing growth models.

The results of our EXAFS study of annealing the $n = 2$ ALS samples have been discussed in detail elsewhere.[51] Briefly, in conjunction with Raman and x-ray diffraction, they show that strain in the Ge layer causes initial interdiffusion four orders of magnitude higher than that for diffusion of Ge into Si after relaxation has occurred (i.e., as measured after long anneals).[51,64,65] The Ge-Si bond begins to relax the same time as the diffusion occurs. Such a quantitative examination of the local structure is critical to improving our understanding of the initial stages of relaxation. It would have been difficult to determine by any other means.

IV. FUTURE DIRECTIONS

We have presented an improved EXAFS analysis procedure based upon simultaneous multiple-file analysis. Its utility for improving the reliability of derived parameters has been illustrated with a study of the thickness dependence of the interface structure of Ge layers buried

in Si. Currently it is adapted only to systems where a Gaussian distance distribution is an appropriate assumption. Even though the constrained fit represents a qualitative improvement, there are a number of concerns that can be justifiably raised with the procedure as it now stands. In an ideally modeled system, the χ^2 for a perfect match between model and experiment should be 1. The fact that our best fits have χ^2 values significantly different from 1 means that a number of aspects of the problem are not correctly accounted for in the model. The use of a nonweighted least-squares procedure is one limitation. A weighted proportional to the statistical precision at each point would emphasize the more accurately known, lower-**k** data, which in this case is more sensitive to the Si-Ge mix and thus should lead to a more stable answer. At the same time the k^1 weighting we have used means that the noisier high-k data is not unduly weighted in the fit. A more significant problem is probably the difficulty of accounting for systematic errors, particularly the neglect of certain aspects of the physical problem in the standard EXAFS formulation (e.g., non-Gaussian distributions) and the dependence of the final answer on aspects of the preparation of the Fourier filtered data.

At present we are constructing procedures to parametrize (and eventually scan) the file preparation steps (energy calibration, background subtraction, k-scale, and R-window selection). While we suspect that a fully automated "turn-key" EXAFS analysis algorithm is as yet unattainable, this will facilitate understanding of systematic errors such as the dependence of the final result on data-file-preparation aspects of the analysis. When combined with scans of the initial parameters and subsequent graphical analysis like those in Figs. 4–7, a much better understanding of the dependence of the final answer on each analysis step and, thus, a better estimation of absolute error, will become possible. It is not yet clear how one could combine these considerations into a better formula to which optimal fits would produce $\chi^2=1$.[29]

A qualitative extension of this constrained-fitting procedure, which would be particularly valuable for studies of Si-Ge interfaces, would be a simultaneous analysis of EXAFS from core edges of both elements of a heterobond. While Si K EXAFS studies of Si-Ge interfaces and alloys have been reported,[52–54] no one as yet has carried out a combined Ge K and Si K study. In principle, requiring that R and σ^2 values be the same as viewed from each side of the bond (e.g., that $R_{\text{Si-Ge}}$ and σ^2(Si-Ge) from Si K EXAFS are identical to the values derived from Ge K EXAFS) should provide a very powerful constraint on the analysis. Of course, one must be careful to correctly establish the constraint, since the DW and E_0 parameters are relative to those for the model, and these will differ. We have begun a program of Si K-edge measurements[66] but have not yet obtained data of sufficient quality to advance the analysis of the Si-Ge interface.

Another development will be the introduction of analytical relationships among parameters, rather than simply requiring sets of parameters to have identical values. Thus, in a series where one expects a near-linear variation of, e.g., bond length as a function of composition, the fit could adjust the two parameters of a linear equation rather than four individual bond lengths. It should also be possible to include a provision for non-Gaussian distance distributions.

The constrained multiple-file analysis, in conjunction with exploration of the fit surface, has provided much greater confidence in the results for both the thickness dependence (this work) and the evolution of a thin Ge_2 layer as a function of annealing time.[51] We believe EXAFS measurements on a finer mesh of samples (both variable thickness and anneal procedures) will allow improved understanding of the mechanisms for epitaxial growth of Si-Ge interfaces and their transformation during thermal processing. Such understanding will be extremely beneficial in being able to meet the demands of device designers concerning epitaxial interface quality and subsequent processability.

V. SUMMARY

Based on the measurements described above, the following conclusions have been drawn regarding this series of Si-Ge ALS samples. For $n<4$ the Ge-Ge bond length is not that of bulk Ge as has been reported for strained alloy layers but, rather, it is that of a fully strained pure Ge layer. The Si-Ge is distinctly shorter than the Ge-Ge distance. As n increases, the Ge-Ge distance relaxes in the direction of higher values.

ACKNOWLEDGMENTS

Financial support was provided by NSERC (Canada) and the Ontario Centre for Materials Research (OCMR). Acknowledgement is made to the donors of the Petroleum Research Fund, administered by the ACS, for partial support of this research. We thank the dedicated staff scientists and operators at CHESS for their assistance. CHESS is supported by the National Science Foundation. Useful discussions with C. Dharma-wardana and E. D. Crozier are acknowledged. We thank K. Sakamoto for providing a $SiGe_2Si$ single-layer sample for comparison measurements. The assistance of K. McCuaig in synthesis of the $Ge[Si(CH_3)]_4$ model compound and H. G. Labbé for the Raman measurement is acknowledged.

[1]P. A. Lee, P. H. Citrin, P. Eisenberger, and B. M. Kincaid, Rev. Mod. Phys. **53**, 769 (1981).

[2]*X-ray Absorption: Principles, Techniques and Applications of EXAFS and XANES,* edited by D. Konigsberger and R. Prins (Academic, New York, 1988).

[3]E. Zanazzi and F. Jona, Surf. Sci. **62**, 61 (1977); J. B. Pendry, J. Phys. C **13**, 1937 (1980); S. Anderson and J. B. Pendry, *ibid.* **13**, 3547 (1980).

[4]*Spectrscopy of Semiconductor Microstructure,* edited by G. Fasol, A. Fasolino, and P. Lugli (Plenum, New York, 1989).

[5]J. C. Woicik, C. E. Bouldin, M. I. Bell, J. O. Cross, D. J. Tweet, B. D. Swanson, T. M. Zhang, L. B. Sorensen, C. A. King, J. L. Hoyt, P. Pianetta, and J. F. Gibbons, Phys. Rev. B **43**, 2419 (1991).

[6] *Silicon Molecular Beam Epitaxy,* edited by J. C. Bean and E. Kasper (Chemical Rubber Company, Boca Raton, FL 1988).
[7] M. Zinke-Allmang, L. C. Feldman, S. Nakahara, and B. A. Davidson, Phys. Rev. B **39**, 7848 (1989).
[8] J. Bevk, J. P. Mannaerts, L. C. Feldman, B. A. Davidson, and A. Ourmazd, Appl. Phys. Lett. **49**, 286 (1986).
[9] A. A. Williams, J. M. C. Thornton, J. E. MacDonald, R. G. van Silfhout, J. F. van der Veen, M. S. Finney, A. D. Johnson, and C. Norris, Phys. Rev. B **43**, 5001 (1991).
[10] Y.-W. Mo, D. E. Savage, B. Swartzentruber, and M. G. Lagally, Phys. Rev. Lett. **65**, 1020 (1990).
[11] A. Ourmazd and J. C. Bean, Phys. Rev. Lett. **55**, 765 (1985).
[12] D. J. Lockwood, K. Rajan, E. W. Fenton, J-.M. Baribeau, and M. W. Denhoff, Solid State Commun. **61**, 465 (1987).
[13] F. K. LeGoues, V. P. Kesan, and S. S. Iyer, Phys. Rev. Lett. **64**, 40 (1990).
[14] F. K. LeGoues, V. P. Kesan, S. S. Iyer, J. Tersoff, and R. Tromp, Phys. Rev. Lett. **64**, 2038 (1990).
[15] E. Muller, H. U. Nissen, M. Ospelt, and H. von Kanel, Phys. Rev. Lett. **63**, 1819 (1989).
[16] D. E. Jesson, S. J. Pennycook, and J-M. Baribeau, Phys. Rev. Lett. **66**, 750 (1991).
[17] J. L. Martins and A. Zunger, Phys. Rev. Lett. **56**, 1400 (1986).
[18] P. B. Littlewood, Phys. Rev. B **34**, 1363 (1986).
[19] S. Ciraci and I. P. Batra, Phys. Rev. B **38**, 1835 (1988).
[20] M. Copel, M. C. Reuter, E. Kaxiras, and R. Tromp, Phys. Rev. Lett. **63**, 632 (1989).
[21] T. P. Pearsall, CRC Crit. Rev. Solid State Mater. Sci. **15**, 551 (1989).
[22] J-M. Baribeau, D. J. Lockwood, M. W. C. Dharma-wardana, N. L. Rowell and J. P. McCaffrey, Thin Solid Films **183**, 17 (1989).
[23] J-M. Baribeau, D. J. Lockwood, T. E. Jackman, P. Aebi, T. Tyliszczak, and A. P. Hitchcock, Can. J. Phys. **69**, 246 (1991).
[24] D. J. Lockwood and J-M. Baribeau (unpublished).
[25] D. J. Lockwood, M. W. C. Dharma-wardana, J-.M. Baribeau, and D. C. Houghton, Phys. Rev. B **35**, 2243 (1987).
[26] D. J. Lockwood, Proc. SPIE **1336**, 13 (1990).
[27] M. W. C. Dharma-wardana, G. C. Aers, D. J. Lockwood, and J-M. Baribeau, Phys. Rev. B **41**, 5319 (1990).
[28] D. J. Lockwood and J-M. Baribeau, in *Light Scattering and Semiconductor Structures,* edited by D. J. Lockwood and J. F. Young (Plenum, New York, 1991), p. 197.
[29] F. W. Lytle, D. E. Sayers, and E. A. Stern, Physica B **158**, 701 (1989).
[30] A. G. McKale, B. W. Veal, A. P. Paulikas, S. K. Chan, and G. S. Knapp, J. Am. Chem. Soc. **110**, 3763 (1988).
[31] J. Mustre, Y. Yacoby, E. A. Stern, and J. J. Rehr, Phys. Rev. B **42**, 10 843 (1990).
[32] B. K. Teo and P. A. Lee, J. Am. Chem. Soc. **101**, 2816 (1979).
[33] J. W. Cook and D. E. Sayers, J. Appl. Phys. **52**, 5024 (1981).
[34] S. P. Hershfeld and T. L. Einstein, Phys. Rev. B **29**, 1048 (1984).
[35] B. A. Bunker and E. A. Stern, Phys. Rev. B **27**, 1017 (1983).
[36] M. B. Stearns, Phys. Rev. B **25**, 2382 (1982).
[37] E. D. Crozier, J. J. Rehr, and R. Ingalls, in *X-ray Absorption: Principles, Techniques and Applications of EXAFS and XANES* (Ref. 2), Chap. 9; B. Bunker, Nucl. Instrum. Methods **207**, 437 (1983).
[38] P. A. Lee and G. Beni, Phys. Rev. B **25**, 2862 (1977); J. B. A. D. van Zon, D. C. Koningsberger, H. F. van't Blik, and D. E. Sayers, J. Chem. Phys. **82**, 5742 (1985).
[39] N. S. Chiu and S. H. Bauer, J. Phys. Chem. **92**, 565 (1988).
[40] E. D. Crozier, Physica B **158**, 14 (1989).
[41] S. J. Gurman, J. Phys. C **21**, 3699 (1988).
[42] G. Martens, P. Rabe, N. Schwentner, and A. Werner, Phys. Rev. Lett. **39**, 1411 (1977).
[43] M. Choi, J. Budnick, G. H.Hayes, D. M. Pease, S. M. Heald, D. E. Sayers, and R. Hasegawa, Phys. Rev. B **36**, 4613 (1987).
[44] W. Zhou, M. Paesler, and D. E. Sayers, Phys. Rev. B **43**, 2315 (1991).
[45] T. M. Hayes and J. B. Boyce, Solid State Phys. **37**, 173 (1982).
[46] F. Aliotta, G. Galli, G. Maisano, P. Migliardo, C. Vasi, F. Wanderlingh, Nuovo Cimento **2D**, 103 (1983); R. Duhlev, I. D. Brown, T. Tyliszczak, and A. P. Hitchcock (unpublished).
[47] B. K. Teo, M. R. Antonio, and B. A. Averill, J. Am. Chem. Soc. **105**, 3751 (1983).
[48] H. Oyanagi, T. Sakamoto, K. Sakamoto, T. Matsushita, T. Yao, and T. Isheguro, J. Phys. Soc. Jpn. **57**, 2086 (1988); H. Oyanagi, T. Sakamoto, K. Sakamoto, H. Yamaguchi, and T. Yao, in *Extended Abstracts of the 21st Conference on Solid State Developments and Materials, Tokyo, 1989* (The Business Center for Academic Society of Japan, Tokyo, 1989), p. 509; H. Oyanagi, T. Sakamoto, K. Sakamoto, H. Yamaguchi, Y. Kuwahara, T. Matsushita, and T. Yao, *Proceedings of the Extended Absorption Fine Structure 6* (Oxford University Press, London, in press).
[49] C. Bouldin, Physica B **158**, 596 (1989).
[50] P. Aebi, T. Tyliszczak, A. P. Hitchcock, T. E. Jackman, and J-M. Baribeau, J. Vac. Sci. Technol. A **9**, 907 (1991).
[51] T. E. Jackman, J-M. Baribeau, D. J. Lockwood, P. Aebi, T. Tyliszczak, and A. P. Hitchcock, Phys. Rev. B **45**, 13 591 (1992).
[52] L. Incoccia, S. Mobilio, M. G. Proietti, P. Fiorini, C. Giovannella, and F. Evangelisti, Phys. Rev. B **31**, 1028 (1985).
[53] A. Filipponi, P. Fiorini, F. Evangelisti, A. Balerena and S. Mobilio, J. Phys. (Paris) Colloq. **47**, C8-357 (1986).
[54] F. Sette, B. Abeles, L. Yang, A. A. MacDowell, C. H. Richardson, and D. Norman, Phys. Rev. B **37**, 2749 (1988).
[55] M. Ichimura, Y. Nishino, H. Kajiyama, and T. Wada, Jpn. J. Appl. Phys. **29**, 842 (1990).
[56] L. Brillouin, *Science and Information Theory,* 2nd ed (Academic, New York, 1962).
[57] A. Erbil, G. S. Cargill III, R. Frahm, and R. F. Boehme, Phys. Rev. B **37**, 2450 (1988); W. T. Elam, J. P. Kikland, R. A. Neiser, and P. D. Wolf, Phys. Rev. B **38**, 2 (1988).
[58] T. Tyliszczak, A. P. Hitchcock, and T. E. Jackman, J. Vac. Sci. Technol. A **8**, 2020 (1990).
[59] T. Tyliszczak and A. P. Hitchcock, Physica B **158**, 335 (1989).
[60] Compound prepared as described in A. G. Brook, F. Abdesaken, H. Soellradl, J. Organomet. Chem. **9**, 299 (1986).
[61] L. Parkanyl, C. Hernandez, and K. H. Pannell, J. Organomet. Chem. **301**, 145 (1986); K. H. Pannell, R. N. Kapoor, R. Raptis, L. Parkanyi, and V. Fulop, *ibid.* **384**, 41 (1990).
[62] S. J. Pennycook (private communication).
[63] S. de Gironcoli, P. Giannozzi, and S. Baroni, Phys. Rev. Lett. **66**, 2116 (1991).
[64] J-M. Baribeau, R. Pascual, and S. Saimoto, Appl. Phys. Lett. **57**, 1502 (1991); R. Pascual, S. Saimoto, and J-M. Baribeau, Can. J. Phys. **69**, 241 (1991).
[65] S. S. Iyer, J. C. Tsang, M. W. Copel, P. R. Pukite, and R. M. Tromp, Appl. Phys. Lett. **54**, 219 (1989).
[66] The Si *K* studies are being carried out at the new double crystal monochromator of the Canadian Synchrotron Radiation Faciltiy at the University of Wisconsin-Madison facility (SRC, Stoughton, WI); B. X. Yang, F. Middleton, B. Olssen, G. M. Bancroft, J. M. Chen, T. K. Sham, K. H. Tan, and D. Wallace, Rev. Sci. Instrum. **63**, 1 (1992).